Improved target illumination at Ludvika mines of Sweden through seismic-interferometric surface-wave suppression

Balestrini, Florencia; Draganov, Deyan; Malehmir, Alireza; Marsden, Paul; Ghose, Ranajit

Important note
To cite this publication, please use the final published version (if applicable).
Please check the document version above.

Improved target illumination at Ludvika mines of Sweden through seismic-interferometric surface-wave suppression

Florencia Balestrini[1]*, Deyan Draganov[1], Alireza Malehmir[2], Paul Marsden[3] and Ranajit Ghose[1]

[1]*Department of Geoscience and Engineering, Delft University of Technology, Delft, The Netherlands,* [2]*Department of Earth Sciences, Uppsala University, Uppsala, Sweden, and* [3]*NIO (Nordic Iron Ore AB), Ludvika, Sweden*

ABSTRACT

In mineral exploration, new methods to improve the delineation of ore deposits at depth are in demand. For this purpose, increasing the signal-to-noise ratio through suitable data processing is an important requirement. Seismic reflection methods have proven to be useful to image mineral deposits. However, in most hard rock environments, surface waves constitute the most undesirable source-generated or ambient noise in the data that, especially given their typical broadband nature, often mask the events of interest like body-wave reflections and diffractions. In this study, we show the efficacy of a two-step procedure to suppress surface waves in an active-source reflection seismic dataset acquired in the Ludvika mining area of Sweden. First, we use seismic interferometry to estimate the surface-wave energy between receivers, given that they are the most energetic arrivals in the dataset. Second, we adaptively subtract the retrieved surface waves from the original shot gathers, checking the quality of the unveiled reflections. We see that several reflections, judged to be from the mineralization zone, are enhanced and better visualized after this two-step procedure. Our comparison with results from frequency-wavenumber filtering verifies the effectiveness of our scheme, since the presence of linear artefacts is reduced. The results are encouraging, as they open up new possibilities for denoising hard rock seismic data and, in particular, for imaging of deep mineral deposits using seismic reflections. This approach is purely data driven and does not require significant judgment on the dip and frequency content of present surface waves, which often vary from place to place.

Key words: Data processing, Ludvika mines, Seismic Interferometry, Seismics, Surface waves.

INTRODUCTION

The main aim of a mineral exploration programme is to discover new deposits in a cost-effective and environmentally friendly manner. The exploration process usually starts by looking for mineral targets that can be of economic interest as observed in surface and aerial measurements and by sampling geological areas that have a potential to yield commercially viable concentrations of minerals. It is important to determine if the exploration project is likely to be profitable. To do so, it is necessary to know the full extent of the mineralized horizons and their geometry, as well as their host rock.

The Bergslagen mineral district in central Sweden is characterized by several multi-commodity mineral deposits. In particular, the district is known by its iron oxide apatite-bearing

*E-mail: f.i.balestrini@tudelft.nl
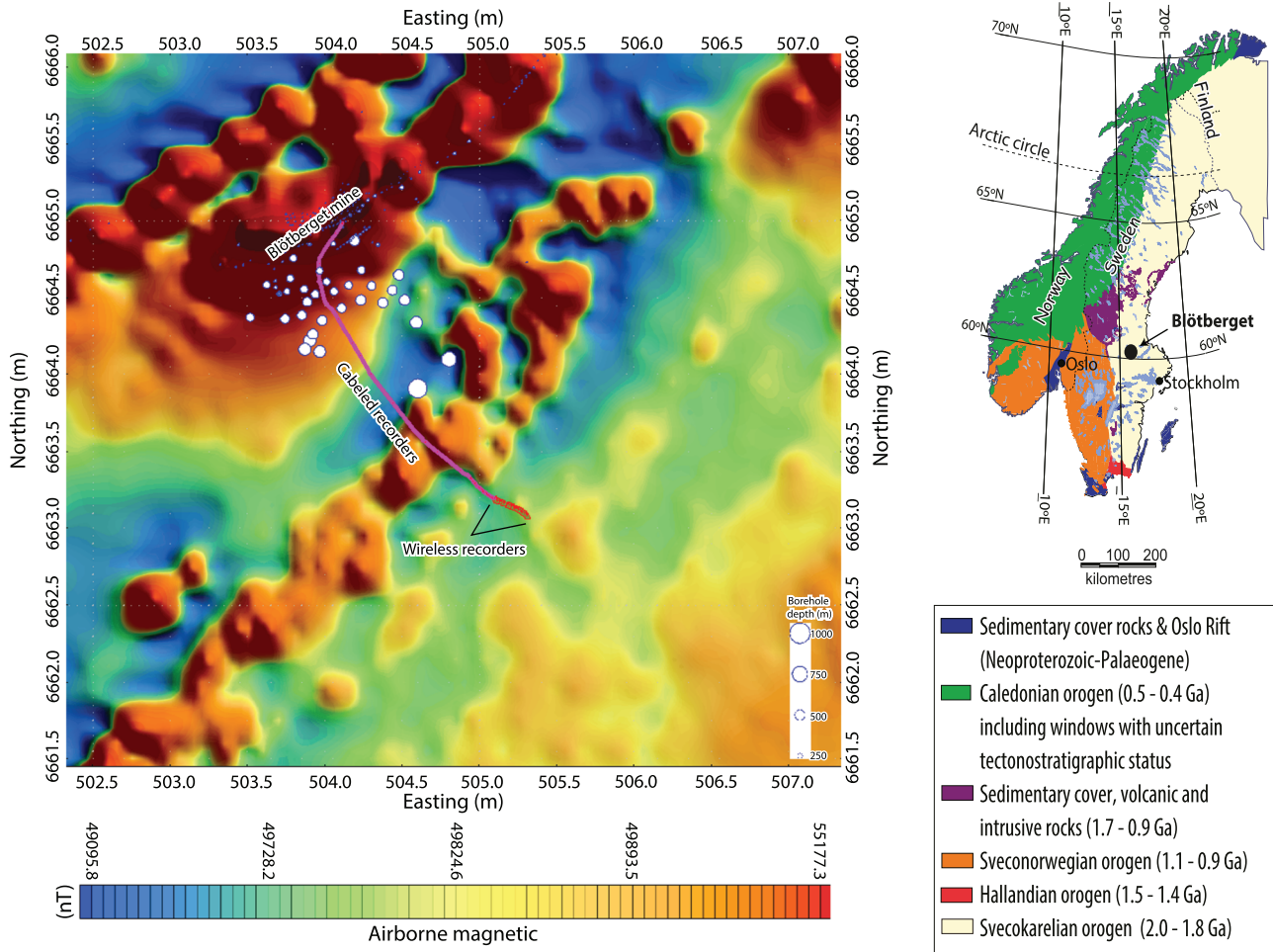Data subject to third party restrictions.

Figure 1 Magnetic map of the Blötberget mine showing the signature of the mineralization zone and the location of the seismic profile (magenta line) used in this study. The white and blue circles indicate positions of boreholes used for downhole logging.

deposits, since they are the most abundant and economically important natural resources in this area (Stephens 2009). Our study area is located in Blötberget, part of the Bergslagen district and the Ludvika mines (Fig. 1). The Blötberget iron oxide deposit was exploited up to a depth of approximately 240 m, until the mining operation stopped in the year 1979 due to the low market price of iron ore (Malehmir *et al.* 2017). However, new favourable market conditions accompanied by the increase of the iron-ore price a few years ago (2011–2014), which is currently between four and five times higher, encouraged a number of initiatives for a reassessment of the deposit and possible generation of new targets (Maries *et al.* 2017a; Yehuwalashet and Malehmir 2018).

Currently, the ore deposits being mined are characterized by shallow depths due to the ease of their exploration and

extraction. But as these ore deposits are already discovered, new ore discoveries in the near future would be at relatively larger depths. To explore for such deeper targets effectively, efficient and high-resolution methods are needed. In this regard, an ever-increasing utilization of seismic methods in mineral exploration and mine planning is noteworthy (e.g. Eaton, Bernd and Salisbury 2003; Koivisto *et al.* 2012; Malehmir *et al.* 2012 and references therein; Malinowski, Schetselaar and White 2012; Manzi *et al.* 2012; Buske, Bellefleur and Malehmir 2015 and references therein). There is a significant growth in the last few years in the use of these methods due to their capability of exploring relatively greater depths (e.g. 850 m and deeper for our case) with higher resolution compared to other geophysical methods, making them more convenient for deep

mineral exploration. However, because the seismic impedance contrast between the mineral deposit and the embedding medium is commonly low, a good signal-to-noise ratio is needed in order to enable better imaging and characterization of the targets.

In exploration seismology, surface waves (sometimes also referred to as ground roll) constitute a form of source-generated energy. These waves propagate along the Earth's surface and are generally the most energetic arrivals in land seismic records. Surface waves are strongly influenced by the elastic properties of the subsurface and, therefore, contain information that could be useful to characterize the medium they propagate through (Shearer 2009). However, when one aims to use reflected body waves for imaging, the surface waves are considered noise because they often mask the reflection events of interest, especially in high-noise, near-mine environments. That is why great efforts are required to suppress the surface waves (Roots, Calvert and Craven 2017), especially when the overburden is thick or has a large impedance contrast with the underlying crystalline bedrock.

Conventionally, surface waves can be suppressed already in the field by deploying receiver arrays instead of single stations, or in the recorded data during processing using suitable filters in the frequency-wavenumber (f-k) or frequency-offset (f-x) domains (Yilmaz 2001). Such filtering methods can be ineffective when the surface waves occupy the same regions in the f-k or f-x domains as the reflected body waves that we wish to preserve (Xue, Aoki and Schuster 2009; Konstantaki *et al.* 2015a). Additionally, an incorrect choice of the f-k or f-x filter parameters may lead to the appearance of artefacts, affecting the quality of the seismic images. In this study, we illustrate the application of a novel method of surface-wave noise suppression for deep mineral exploration through utilization of seismic interferometry (SI). Using SI, we estimate the surface-wave energy between receivers in a purely data-driven manner. We then subtract the retrieved surface-wave energy in an adaptive way from the original data to obtain shot gathers with higher signal-to-noise ratio. These results can be then used in seismic reflection-data processing and imaging. This technique has been referred to as interferometric surface-wave suppression by a number of authors studying the application of SI for the purpose of surface-wave suppression. Dong, He and Schuster (2006) and Halliday *et al.* (2010) showed results in the context of hydrocarbon exploration, whereas Konstantaki *et al.* (2015b) and Liu, Draganov and Ghose (2018) showed results for near-surface applications. These studies suggest how surface waves between two receivers could be retrieved by cross-correlating recorded traces at these receivers,

and how subsequently these retrieved responses could be used for surface-wave suppression. These authors also illustrated that, compared to other surface-wave suppression methods, the interferometric method can naturally predict the surface waves in the shot gather without the use of any *a priori* velocity model and can suppress the surface waves through the use of a least-square matching filter. Nevertheless, to date the number of applications of this technique to noisy field seismic data is rather limited and, to the best of our knowledge, there are no applications in hard rock mining environments reported so far.

In this study, we apply interferometric surface-wave suppression for imaging the iron oxide mineralization in Blötberget, using seismic reflection data acquired in 2016 (Malehmir *et al.* 2017; Maries *et al.* 2017b). This study is part of a larger effort in exploring the potential of the acquired seismic dataset at the site for delineating the deep iron oxide mineralization zone (Malehmir *et al.* 2019).

BLÖTBERGET IRON OXIDE DEPOSIT

The study area, Blötberget in the Ludvika mining area (Fig. 1), is located in Bergslagen in central Sweden, one of the major mineral districts in the country. The mineralization in Bergslagen comprises a banded-iron formation, skarn-type iron oxide deposits and apatite-rich iron oxide deposits, with the latter deposits accounting for more than 40% of the iron ore produced in the country (Magnusson 1970; Stephens *et al.* 2000). Bergslagen has always been economically important, but due to the low metal prices in the 1980–1990s, output from the mines decreased or even stopped, leading to just a few mines operating in the region. In particular, Blötberget is well known for its rich and high-quality iron oxide deposit. However, the mining operation ceased in 1979, with most of the mining taking place at approximately 240 m depth at the time of closure. Nowadays, there is a renewed interest in exploring and mining this deposit, but also similar ones in the area, due to accessibility to the market and the recent advancements made in low-cost mining and metallurgical technologies. A number of recent works in the Blötberget and neighbouring areas are aimed at achieving a better understanding of the mineralization at depth, as well as at technological developments (e.g. Place *et al.* 2015; Malehmir *et al.* 2017; Yehuwalashet and Malehmir 2018).

The mineralization in Blötberget consists of magnetite and hematite. Additionally, apatite and small amounts of quartz and calc-silicate minerals are present. The deposit contains approximately 55 Mt of iron with an average iron

content of 41%, dominantly from magnetite, but it is also composed of several horizons where hematite is rich or notably present. The hematite ores are less massive than the magnetite ones, and their skarn host-rock mineralogy is slightly different, containing more quartz and feldspar. The origin of the iron oxide apatite-bearing deposit is considered to be syn-volcanic, although this is disputed, with a new study favouring a magmatic to high-temperature hydrothermal origin (Jonsson *et al.* 2013). The mineralized units dip moderately (about 45°) towards the southeast down to 500 m, at which depth they become gently dipping until the known depth of approximately 800–850 m (known from historical one-inch diameter holes; Maries *et al.* 2017a). Deeper than that level, the mineralization units still need to be explored (Malehmir *et al.* 2017; Maries *et al.* 2017a).

SEISMIC DATA ACQUISITION

The two-dimensional reflection seismic dataset used in this study was acquired in a field campaign in 2016 that used both wireless and cabled recorders (Maries *et al.* 2017b). Figure 1 shows the seismic profile (magenta crooked line), along which the sources and receivers were positioned. The white and blue circles indicate the position of historical boreholes in the area. The profile was designed such that it intersects perpendicularly the strike direction of the known mineralization in order to keep any possible cross-dip and three-dimensional scattering effects to a minimum. The aim of the 2016 survey was to delineate any potential depth extension of the mineralization towards the southeast, which could not be achieved in an earlier survey conducted in 2015 using mainly a land-streamer system. The landstreamer survey was characterized by a lower common midpoint (CMP) fold coverage and as a result could only confirm the known mineralization (Malehmir *et al.* 2017). The 2016 survey consisted of two profiles. One of them was positioned along the profile of the 2015 survey, but only north of road 50. This 2016 profile used cabled units and 24 wireless units; the latter was planted in the southern part of the profile. The second profile, shorter and perpendicular to the first profile, used only wireless units. The second profile is not the focus of this study. The spacing between receivers as well as the spacing between shots was 5 m. A 500-kg Bobcat drophammer was used as the seismic source.

Markovic *et al.* (2019) showed the conventional processing results for this dataset merged with the 2015 dataset in order to improve the CMP fold and handle the low signal-to-noise ratio of the data in the area.

SEISMIC INTERFEROMETRY WITH ACTIVE SOURCES FOR SURFACE-WAVE RETRIEVAL

Seismic interferometry (SI) generally refers to the principle of retrieving seismic responses from virtual sources by cross-correlating seismic observations at different receiver locations. One can distinguish between controlled-source and passive SI (Wapenaar, Draganov and Robertson 2008). Controlled-source SI refers to the process of retrieving the response between two receivers *A* and *B* as if there was a source at one of the receiver locations. This process is carried out, most commonly, by cross-correlating the recordings at the two receivers and stacking the cross-correlations over all available controlled sources (Wapenaar and Fokkema 2006).

For an active-source seismic survey, the retrieved response between two receivers at positions $\mathbf{x}_A$ and $\mathbf{x}_B$ can be written as (Halliday *et al.* 2007)

$$\hat{u}(\mathbf{x}_B, \mathbf{x}_A, \omega) + \hat{u}^*(\mathbf{x}_B, \mathbf{x}_A, \omega) \approx \sum_{n=1}^{N} \hat{u}(\mathbf{x}_B, \mathbf{x}_n, \omega)$$
$$\times \hat{u}^*(\mathbf{x}_A, \mathbf{x}_n, \omega), \tag{1}$$

where $\hat{u}(\mathbf{x}_B, \mathbf{x}_n, \omega)$ is the frequency-domain response, as indicated by the hat (^) above *u*, of a recording at receiver $\mathbf{x}_B$ from a source at $\mathbf{x}_n$; the asterisk (*) denotes complex conjugation in the frequency domain, which corresponds to a time-reversed version of a quantity in the time domain (i.e. $u(\mathbf{x}_B, \mathbf{x}_A, -t)$ in our case). *N* represents the number of active sources. If an active source emits an impulse, $\hat{u}(\mathbf{x}_B, \mathbf{x}_A, \omega)$ would represent an impulse response. For transient sources, $\hat{u}(\mathbf{x}_B, \mathbf{x}_A, \omega)$ would represent a pressure or a particle velocity recording convolved with the autocorrelation of the sources' time function. Through equation (1), we can turn the receiver at $\mathbf{x}_A$ into a virtual source. If we keep the receiver at $\mathbf{x}_A$ fixed and repeat the correlation and summation process for all other receivers, the retrieved result would approximate a virtual common-source gather with a virtual source located at $\mathbf{x}_A$. The theory of SI requires that the sources effectively surround the receivers and illuminate them homogeneously (Wapenaar and Fokkema 2006). When the receivers are at the surface, that is, $\hat{u}$ represents a particle velocity recording, active sources are required only in the subsurface (Wapenaar and Fokkema 2006). For the usual seismic exploration, the active sources are present at the surface, where they are not required. As a consequence, the retrieved result would contain not only physical arrivals but also spurious contributions to the interferometric estimate like virtual refractions and non-physical reflections (e.g., Mikesell *et al.* 2009; Draganov *et al.* 2010; Draganov, Heller and Ghose 2012; King and Curtis 2012; Draganov *et al.*

Table 1 Steps to suppress surface waves and process seismic reflection data to obtain the final stacked section

Step	Instruction
1	Raw data with static corrections applied
2	Band-pass filter 10 – 20 – 40 – 50 Hz
3	Seismic interferometry to estimate the surface waves
4	Adaptive subtraction of the estimated surface waves
5	20 Hz low-cut filter
6	Automatic gain correction
7	Velocity analysis
8	Normal Move Out (NMO) correction
9	Common midpoint/ensemble stack

2013; Boullenger and Draganov 2016; Place and Malehmir 2016). The retrieved physical events include direct body and surface waves, and events that have the correct kinematics of reflections, with the latter obtained from cross-correlation between two consecutive orders of free-surface multiples. These

events with kinematics of reflections are characterized by amplitudes and wavelet phases that are different from those that would be recorded from an active source at the position of the virtual source. Because of that, they are also referred to as pseudo-physical reflections (Löer *et al.* 2013).

For a laterally homogeneous medium, sources at points in-line with the receivers, whose recordings are to be correlated, will contribute to the retrieval of direct body or surface-wave arrivals. Such points are called stationary. Actually, the main contributions to the retrieved direct body and surface waves come from sources in the Fresnel zone around the stationary points (Snieder 2004) – the so-called stationary-phase region (since the rays from such source positions are nearly parallel, and interfere constructively in the summation). For retrieval of direct (P-, S-, or surface) waves from active sources at the surface, all in-line points are stationary; for retrieval of pseudo- or non-physical reflections and scattered surface waves only a few points are stationary. This way, the result retrieved by SI will be dominated by surface waves. Note that
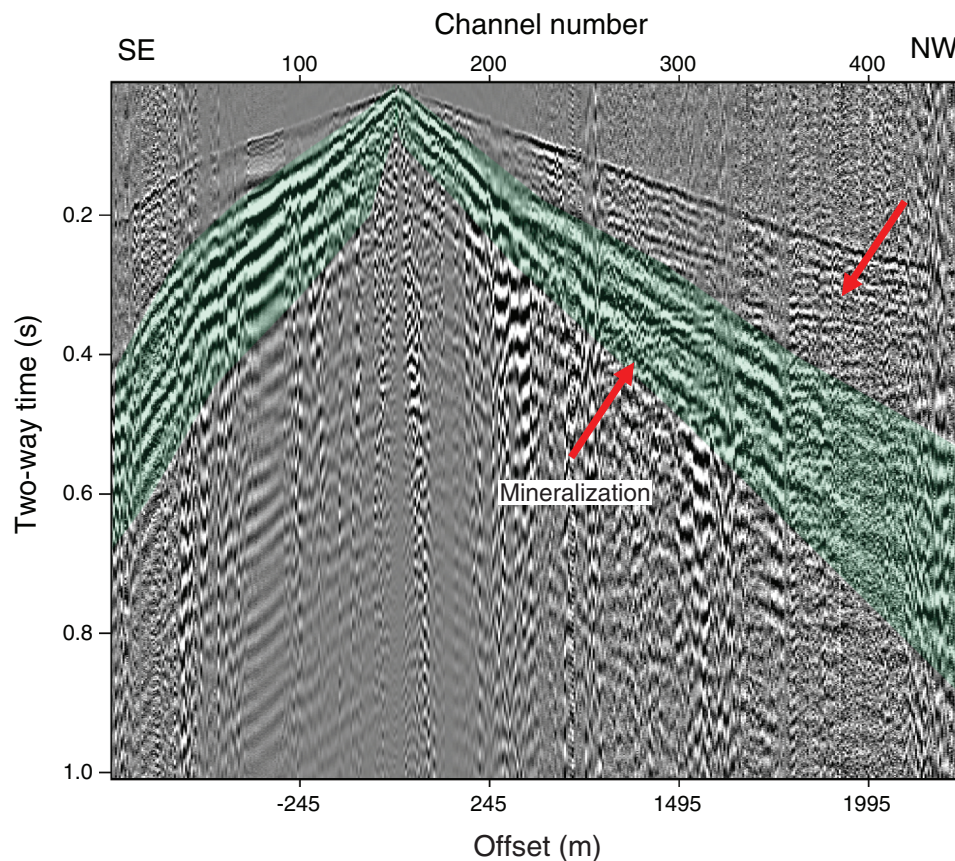

Figure 2 Example of one of the common-shot gather acquired in the field (Ludvika mine), which is used for adaptive subtraction of surface waves. The active source is positioned at station 150. In green, we highlight the surface waves that contaminate the dataset and overlap the mineralization-zone reflections (red arrows).
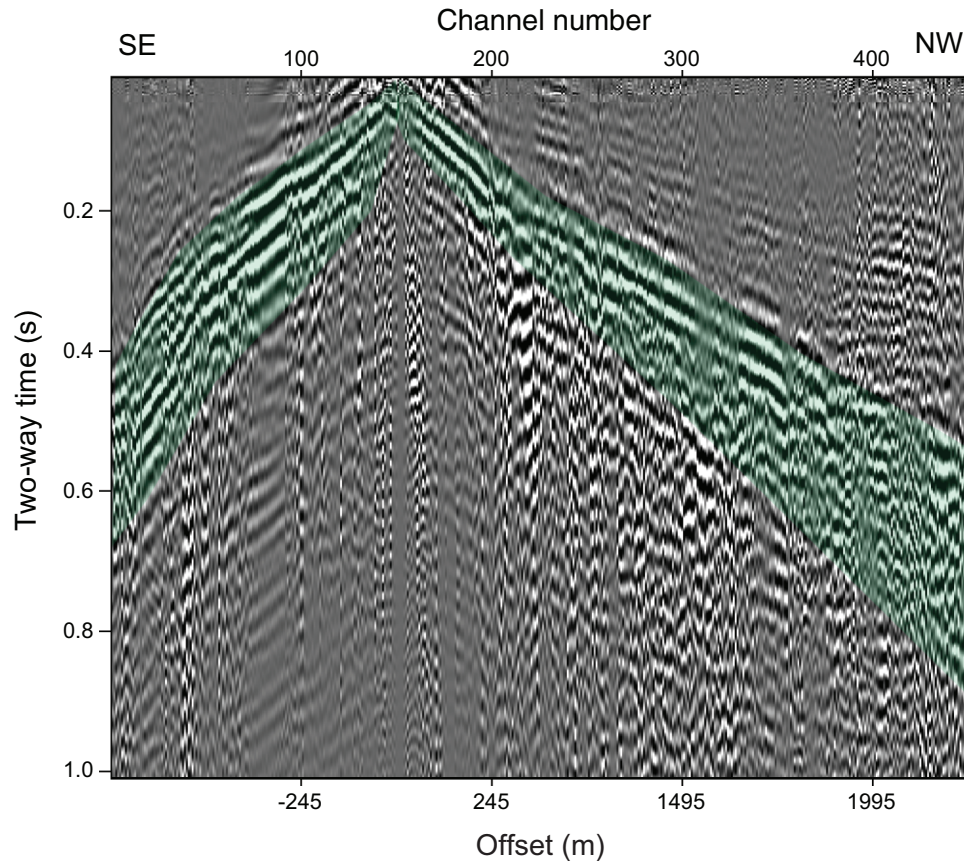
Figure 3 Result of application of SI for retrieval of the response of a virtual source at station 150, to be used as an estimation of the surface-wave energy. Highlighted in green are the retrieved surface waves. It can be seen that they are dominant and well represented.

if we assume that the surface sources mainly contribute to excitement of the fundamental mode, the fundamental mode retrieved by SI would be correct. To retrieve also higher modes, sources in the subsurface are also required (Halliday and Curtis 2008; Kimman and Trampert 2010; van Dalen, Wapenaar and Halliday 2014; van Dalen *et al.* 2015).

If each source position within an exploration survey is located near a receiver position, then a corresponding retrieved virtual source–receiver pair with its estimated surface waves can be found for each active source–receiver pair. These estimates can be adaptively subtracted from the full responses recorded in the field, thus applying interferometric surface-wave suppression (Dong *et al.* 2006; Halliday *et al.* 2010; Konstantaki *et al.* 2015b; Liu *et al.* 2018).

For this study, in order to test the interferometric surface-wave suppression and extraction method on the Blötberget seismic reflection dataset, we isolate and process only the 2016 dataset (magenta line in Fig. 1) since it is the most complete

one, the source and receiver spacing is more regular, and it has no complication due to landstreamer overlaps. All these factors help us avoid challenges in the retrieval of the SI response. From this part of the 2016 dataset, we have not used the northernmost 50 stations for surface-wave retrieval. These stations correspond to the curved part of the 2016 line, for which the active sources are positioned in line only with a few neighbouring receivers, precluding retrieval of direct surface waves. Note that in the particular situation of the Ludvika seismic data, there are receivers at every active-source location. Therefore, we can safely assume that the surface waves are well represented at each position.

ADAPTIVE SUBTRACTION

To perform adaptive subtraction, we estimate a shaping filter that minimizes the difference between the field-recorded data with the surface waves and the surface waves retrieved by the
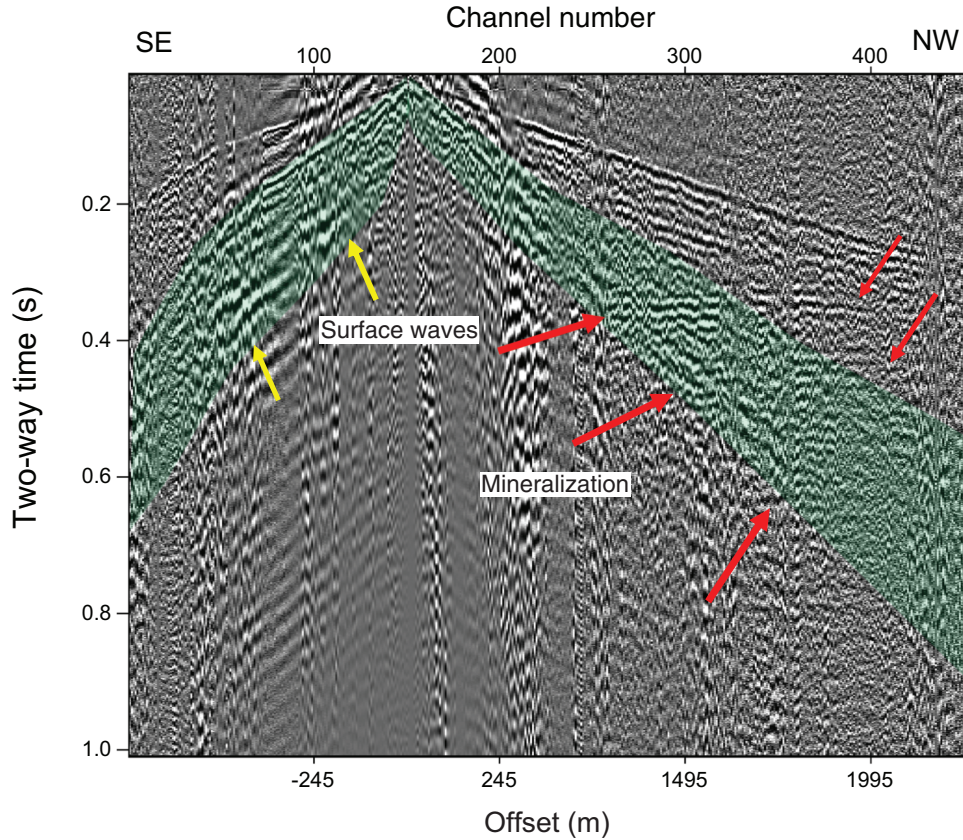
Figure 4 Result after adaptively subtracting the surface waves estimated using SI (Fig. 3) from the original raw data (Fig. 2). The part of the dataset where surface waves were filtered is highlighted in green. Surface waves are suppressed, and the mineralization-zone signature is better illuminated (red arrows). The yellow arrows indicate the remaining surface-wave energy.

application of seismic interferometry (SI) to the field-recorded data. In other words, we solve the following minimization problem for **f** using the least-squares criterion:

$$\min_{f} ||\mathbf{D} - \mathbf{f}\mathbf{D}_{SW}||, \tag{2}$$

where **D** is data with all the information (raw data) and $\mathbf{D}_{SW}$ are the surface waves retrieved by SI applied to **D**. The vertical double bars ($|| \cdot ||$) denote the L2-norm. After obtaining **f**, the data with reflections after suppression of the surface waves ($\mathbf{D}_{refl}$) are obtained by

$$\mathbf{D}_{refl} = \mathbf{D} - \mathbf{f}\mathbf{D}_{SW}, \tag{3}$$

where the multiplication (or convolution in time) between the estimated shaping filter **f** and $\mathbf{D}_{SW}$ leads to $\mathbf{f}\mathbf{D}_{SW}$, which then will be directly subtracted from **D**, giving $\mathbf{D}_{refl}$. We perform different tests by varying the parameters of the adaptive subtraction (e.g. filter length and time and space windows) in order to find the most suitable filter that suppresses the surface waves in an optimal way.

RESULTS

The primary aim of this study is to illustrate the effectiveness of the interferometric surface-wave suppression method, applied to shot gathers of field data (Blötberget 2016 dataset, Maries *et al.* 2017b). For this reason, the data-processing work follows a conventional common midpoint (CMP) stacking workflow after suppression of the surface waves. Table 1 shows a summary of the processing steps that we implement to suppress the surface waves and to process the seismic data in order to obtain the final stacked section. We apply SI to the recorded active-source data in order to estimate the surface-wave energy between the receivers. We then adaptively subtract the retrieved result from the original active data to suppress the surface waves. Prior to surface-wave suppression, the data are subjected to surface-consistent refraction static corrections (Malehmir *et al.* 2017; Markovic *et al.* 2019). Before applying SI, we first filter the data using a band-pass filter between 20 and 45 Hz, by studying the power spectra
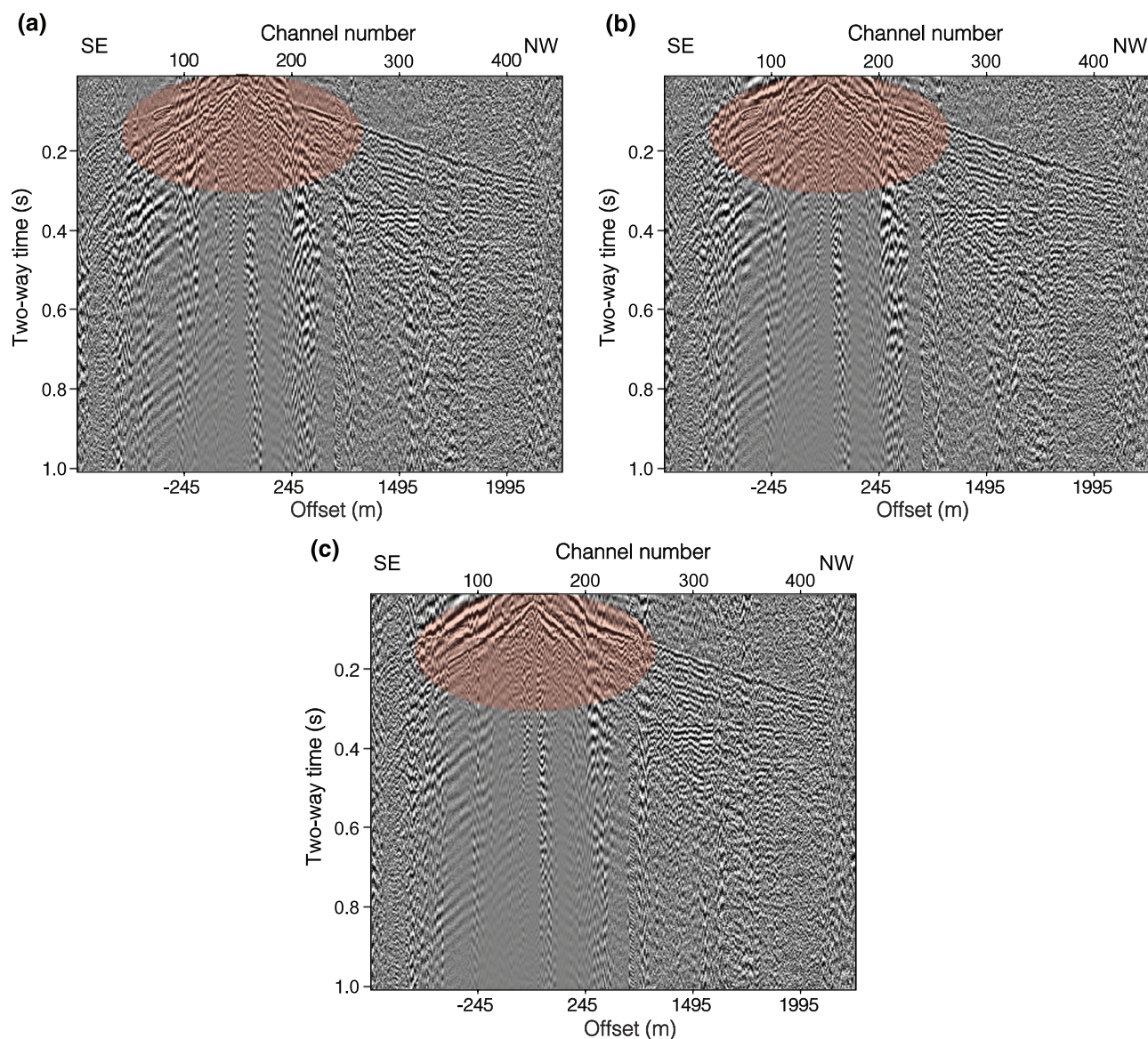
Figure 5 Results after adaptively subtracting the surface waves estimated using SI (Fig. 3) with filter lengths of (a) 50, (b) 100 and (c) 200 samples. The red circles indicate the areas where the filter artefacts arise.

of several shot gathers. The main idea is to reject frequencies that might contain reflection and refraction information in order to have the SI data that retrieve predominantly the surface waves, while having nearly no reflection energy retrieved. Even though the application of SI to data from active sources recorded at the surface naturally suppresses retrieval of body-wave reflections and favours the retrieval of surface waves, this extra step of filtering for reflection attenuation only strengthens the surface-wave retrieval.

Malehmir *et al.* (2017) and Markovic *et al.* (2019) showed in their work the reflections to be interpreted from

the mineralization zone already visible in a raw shot gather; those reflections become more evident after a few prestack processing operations. In Fig. 2, we show an example of a common-source gather as recorded in the field. In green, we highlight the surface waves that contaminate the data and interfere with the known mineralization-related reflections (red arrows). We subject such common-source gathers to band-pass filtering and application of SI. Figure 3 shows the retrieved surface waves after the application of SI. We can note that the retrieved surface waves are dominant and well-represented (green areas). We then perform adaptive
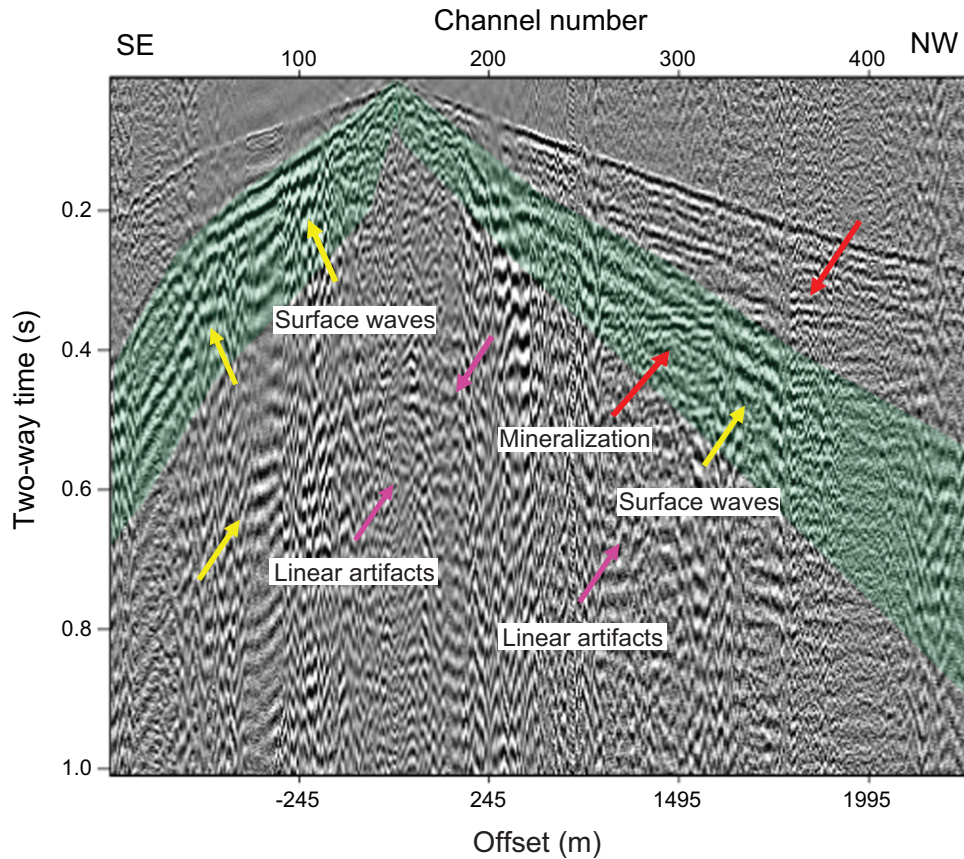
Figure 6 Result showing the suppression of the surface waves using f-k filter on the shot gather shown in Fig. 2. The part of the dataset where surface waves were filtered is highlighted in green. The yellow arrows indicate the remaining surface-wave energy; the magenta arrows point to linear artefacts produced by f-k filter.

subtraction of the result in Fig. 3 from the original data in Fig. 2. Figure 4 shows the result for the same shot gather as in Fig. 2 but after surface-wave removal and after applying a low-cut (20 Hz) filter in order to suppress surface-wave energy remaining. It can be seen that the surface waves are suppressed, and the reflections from the mineralization zone (red arrows) can now be appreciated also at later times. The mineralization signature is represented by reflection events that are hyperbolic in nature, though in this case, they exhibit very little curvature. Figures 5a, 5b, and 5c show the results when using a filter length of 50, 100, and 200 samples, respectively. While changing the time and space window sizes does not generate appreciable variations, we can see that increasing the filter length generates undesired artefacts at earlier times (red circles). Therefore, we apply equation (2) using two-dimensional (2D) windows (spatial width of traces, time length of 0.1 s) with a filter length of 50 samples and an iterative least-squares fit with a conjugate-gradient

algorithm to design the 2D matching filters (Verschuur, Berkhout and Wapenaar 1992; Guitton and Verschuur 2004).

To compare these results with results derived from techniques that are commonly applied, for example, f-k filtering, we perform a power-spectrum analysis and design a polygon filter for each common-shot gather to reject the surface-wave noise. In order to avoid suppression of frequencies representing reflection energy, we constrain the filters between 5 and 60 Hz frequency and 1400 and 3400 m/s velocity. In Fig. 6, we present the result of the application of the designed f-k filter to the common-shot gather in Fig. 2. It can be observed that the surface-wave noise is suppressed as well. However, comparing this result with the one obtained from the interferometric surface-wave suppression, we see that some high-amplitude linear events (yellow arrows in Fig. 6) still remain after the f-k filtering, while they are suppressed in Fig. 4. These linear events represent remaining surface-wave energy, which are
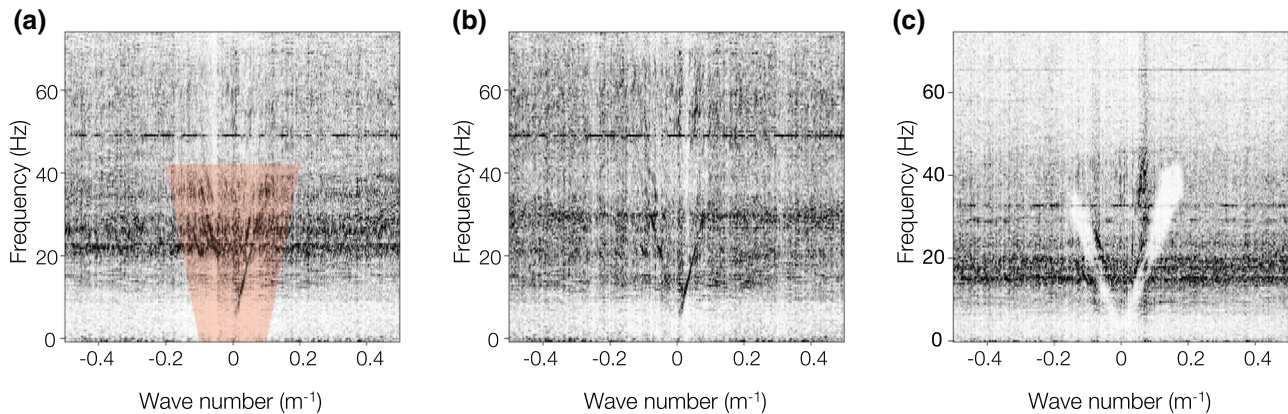
Figure 7 Power spectrum in the frequency-wavenumber domain for (a) the shot gather prior to any processing, (b) the same shot gather after interferometric surface-wave suppression and (c) after surface-wave suppression using f-k filtering. The red area highlights the part where the surface waves are located.

still present as the f-k filter was designed in order to preserve the reflection events of interest. Additionally, the application of the f-k filter has produced some linear artefacts (magenta arrows in Fig. 6). Furthermore, the seismic reflection signature of the mineralization zone is better preserved in Fig. 4. Figures 7a, 7b, and 7c show the power spectrum in the f-k domain for the same shot gather prior to any processing, after interferometric surface-wave suppression, and after f-k filtering, respectively. We can easily identify the surface waves in Fig. 7a (red area); this helps the selection of parameters and the design of the f-k filter as mentioned above. Comparing Figs 7b and 7c, we can see that both methods are effective and help suppress the surface-wave energy. However, it is also clear that the use of f-k filter results in a very aggressive suppression of the frequencies and that, in this case, some artefacts are produced.

After the suppression of the surface waves, we apply a conventional processing sequence to obtain the stacked seismic section. We first apply an automatic gain control for amplitude balancing. After that, we obtain a preliminary stacked section using a one-dimensional (1D) velocity model. The 1D velocity model is built using a root-mean-square velocity obtained for one representative common midpoint (CMP) gather. The CMP spacing is 2.5 m. As expected, the CMP fold increases at the centre of the line where a better illumination is achieved.

Figures 8a, 8b, and 8c show the preliminary unmigrated stacked sections between CMP 270 and CMP 860 using the 1D velocity model obtained from the raw dataset, from the dataset after surface-waves suppression using f-k filtering and from the data after interferometric surface-wave suppression,

respectively. The latter two results already show improved imaging of the mineralization zone (red arrows), which is represented by linear reflectors slightly dipping in the SE direction. It is clear that the high-amplitude and high-frequency linear events, which represent surface-wave noise, are well suppressed in both cases (Figs 8b and 8c). Nevertheless, in case of interferometric surface-wave suppression, the linear noise artefacts are avoided and the mineralization zone is better imaged. Note that even though the interferometric suppression of surface waves performs better, it does not suppress all the surface-wave energy (yellow arrows in Fig. 4). Therefore, we can see steeper linear events in the stacked section that we interpret as surface-wave energy that still remains (yellow arrows in Fig. 8c) at places corresponding to lower CMP fold in the active-source data.

Note further that the seismic stacked section after interferometric surface-wave suppression also reveals a shallower, slightly curved reflector around 0.1 s. Such a reflector is obscured by linear surface-wave noise in Fig. 8a and partly covered by the remaining surface-wave noise (and possibly by f-k filtering artefacts) in Fig. 8b (yellow arrows).

Through generating constant-velocity stacks, we perform a velocity analysis along the line to better image the mineralization-zone reflections and new potential geological structures. This velocity analysis is carried out by generating constant-velocity stacks between 3000 and 8000 m/s with an increment of 100 m/s. After this, we create a 2D velocity model to generate a final stacked section of the subsurface. Only a conventional CMP processing flow is applied, focusing on noise attenuation and signal enhancement by frequency filtering.
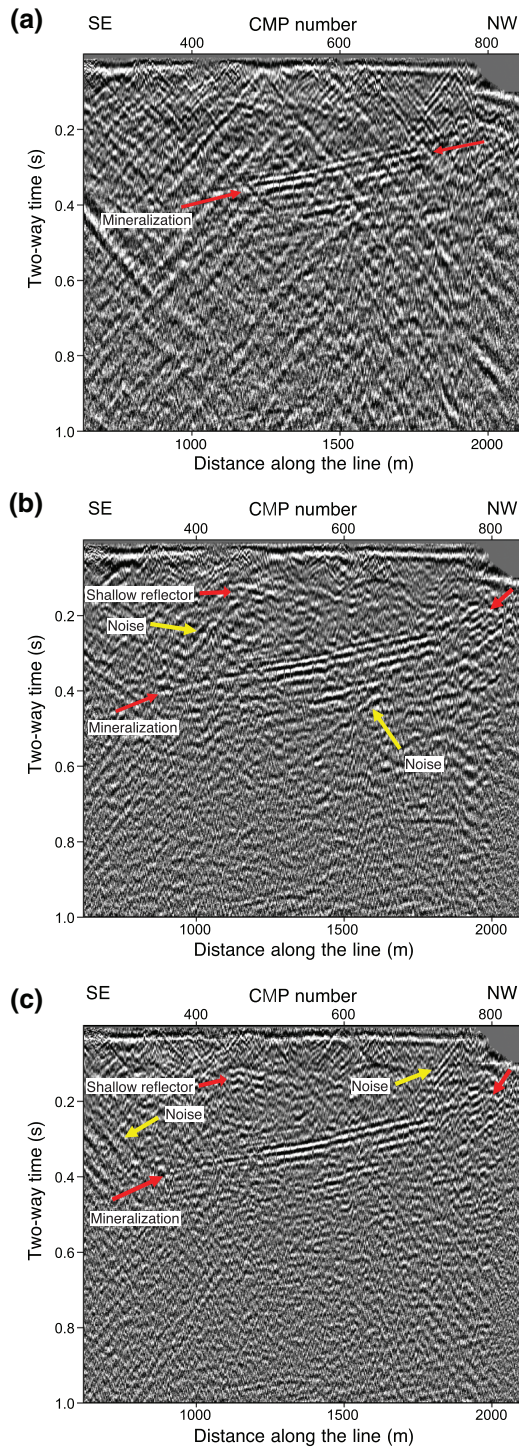
Figure 8 Preliminary unmigrated stacked section, using an 1D velocity model obtained from (a) the raw dataset, (b) the dataset after surface-wave suppression using f-k filter and (c) the dataset after interferometric surface-wave suppression. The red arrows point to the imaged mineralization zone. The yellow arrows mark artefacts generated by f-k filtering and noises that remain in the dataset.
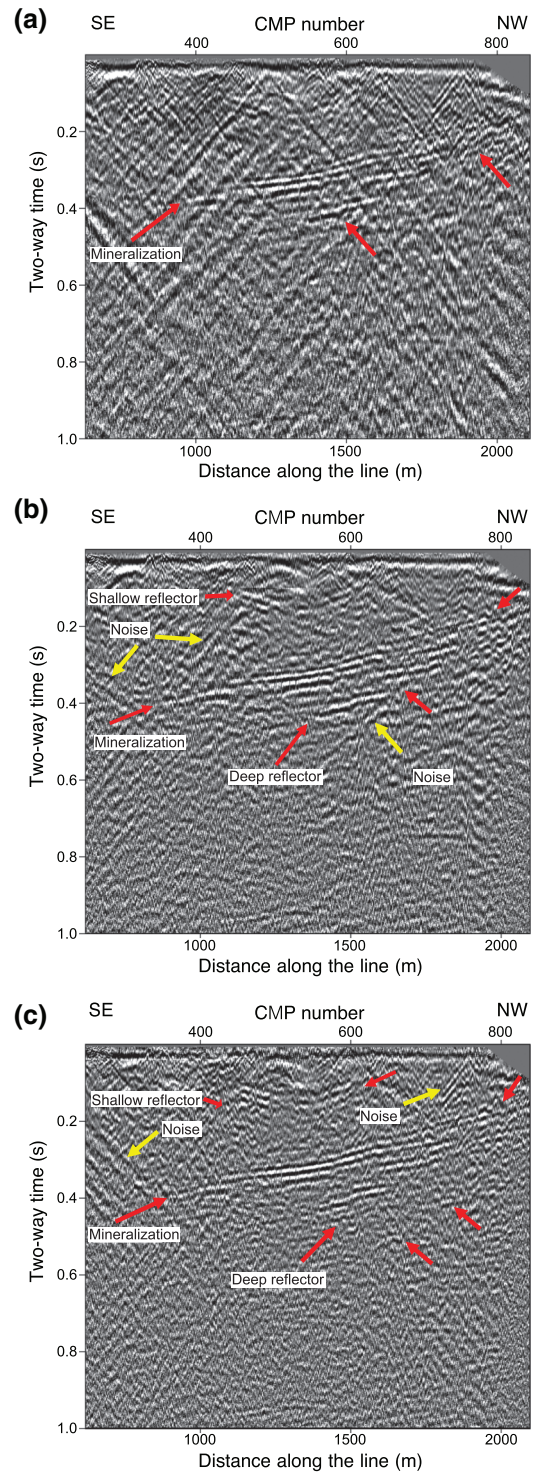
Figure 9 As in Fig. 8, but using the picked 2D velocity model.

Figures 9a, 9b, and 9c show the unmigrated stacked section of the subsurface between CMP 270 and CMP 860 using the picked 2D velocities and applied to the raw dataset, to the data with surface waves suppressed using f-k filtering and to the data after interferometric surface-wave suppression, respectively. Again, we obtain better results for interferometric surface-wave suppression. We can see that the images are clearer for both surface-wave filtering methods, using the same velocity model. However, Fig. 9c, which corresponds to interferometric surface-wave suppression, appears to be less noisy and the mineralization-zone reflectors (red arrows) are more continuous. We notice some linear events in Fig. 9b (yellow arrows) which are artefacts of the f-k filtering due to remaining surface-wave energy. The shallower structures at earlier times (around 0.1 s) are, once again, clearer when interferometric surface-wave suppression is performed.

In order to quantify the comparison between these two techniques, we calculate the signal-to-noise ratio (S/N) for the latter images obtained using the raw data, using the data after f-k filtering for surface-wave suppression, and using the data after interferometric surface-wave suppression. We select two windows from these images, one window to represent the signal (where the mineralization-zone reflections are located), and a second window to represent the background energy (i.e. the noise). We then compute the ratio of their summed squared magnitude to obtain the S/N. We choose both windows between CMP 500 and CMP 630. The window corresponding to the signal is located between 310 and 400 ms, and the window representing the noise is located between 550 and 640 ms. For the image obtained using the raw data, the S/N is 5.25. For the image obtained using the data after f-k filtering for surface-wave suppression, the S/N is 6.03. For the image obtained using the data after interferometric surface-wave suppression, the S/N is 6.94. Therefore, while both surface-wave suppression techniques improve the S/N, the interferometric surface-wave suppression performs clearly better, resulting in a greater improvement of the subsurface image. We perform a second comparison using the same signal window but moving the noise window to a later time, placing it between 850 and 960 ms. In this case, for the image obtained using raw data, the S/N is 7.15. For the image obtained using data after f-k filtering for surface-wave suppression, the S/N is 8.07. For the image obtained using data after interferometric surface-wave suppression, the S/N is 8.09. Again, both surface-wave suppression techniques show increased S/N, but the interferometric surface-wave suppression slightly outperforms the suppression using f-k filtering.

CONCLUSIONS

We have processed a reflection seismic dataset acquired for exploration of the iron oxide mineralization zone in Blötberget, in the Ludvika mining area, south-central Sweden. We applied seismic interferometry to retrieve dominant surface waves between receivers while minimizing the retrieved reflection energy. The retrieved dominant surface waves were then adaptively subtracted from the original data. This resulted in a fully data-driven suppression of surface waves.

We compared stacked sections obtained through the interferometric surface-wave suppression with stacked sections of the raw data (no surface-wave suppression) and with stacked sections where the surface waves were suppressed using frequency-wavenumber filtering. Our results showed not only an improved delineation of the mineralization zone using the interferometric surface-wave suppression but also delineation of new features above and below the known ore deposit.

Our study shows the value of legacy data, and how they could be optimally reprocessed using new seismic techniques in order to allow generation of new mineral exploration targets. It further illustrates the potential of the seismic methods in exploration of deep deposits.

ORCID

Florencia Balestrini 🆔
https://orcid.org/0000-0003-4090-8446
Deyan Draganov 🆔 https://orcid.org/0000-0001-8606-1178
Alireza Malehmir 🆔 https://orcid.org/0000-0003-1241-2988
Ranajit Ghose 🆔 https://orcid.org/0000-0002-9835-7483

REFERENCES

Boullenger B. and Draganov D. 2016. Interferometric identification of surface-related multiples. *Geophysics* **81**, Q41-Q52.

Buske S., Bellefleur G. and Malehmir A. 2015. Introduction to special issue on "hard rock seismic imaging". *Geophysical Prospecting* **63**, 751–753.

Dong S., He R. and Schuster G. 2006. Interferometric prediction and least squares subtraction of surface waves. 76th Annual International Meeting, SEG, Expanded Abstracts, 2783–2786.

Draganov D., Ghose R., Heller K. and Ruigrok E. 2013. Monitoring of changes in velocity and Q in reservoirs using non-physical arrivals in seismic interferometry. *Geophysical Journal International* **192**, 699–709.

Draganov D., Ghose R., Ruigrok E., Thorbecke J. and Wapenaar K. 2010. Seismic interferometry, intrinsic losses and Q-estimation. *Geophysical Prospecting* **58**, 361–373.

Draganov D., Heller K. and Ghose R. 2012. Monitoring CO_2 storage using ghost reflections retrieved from seismic interferometry. *International Journal of Greenhouse Gas Control* **11**, S35–S46.

Eaton D.W., Milkereit B. and Salisbury M. 2003. Seismic methods for deep mineral exploration: mature technologies adapted to new targets. *The Leading Edge* **22**, 580–585.

Guitton A. and Verschuur D.J. 2004. Adaptive subtraction of multiples using the L1-norm. *Geophysical Prospecting* **52**, 27–38.

Halliday D. and Curtis A. 2008. Seismic interferometry, surface waves and source distribution. *Geophysical Journal International* **175**, 1067–1087.

Halliday D., Curtis A., Robertsson J. and van Manen D. 2007. Interferometric surface-wave isolation and removal. *Geophysics* **72**, A69–A73.

Halliday D.F., Curtis A., Vermeer P., Strobbia C., Glushchenko A., van Manen D.J., et al. 2010. Interferometric ground-roll removal: attenuation of scattered surface waves in single-sensor data. *Geophysics* **75**, SA15–SA25.

Jonsson E., Troll V.R., Högdahl K., Harris C., Weis F., Nilsson K.P., et al. 2013. Magmatic origin of giant 'Kiruna-type' apatite-iron-oxide ores in central Sweden. *Scientific Reports* **3**, 1644.

Kimman W.P. and Trampert J. 2010. Approximations in seismic interferometry and their effects on surface waves. *Geophysical Journal International* **182**, 461–476.

King S. and Curtis A. 2012. Suppressing nonphysical reflections in Green's function estimates using source–receiver interferometry. *Geophysics* **77**, Q15–Q25.

Koivisto E., Malehmir A., Heikkinen P., Heinonen S. and Kukkonen I. 2012. 2D reflection seismic investigations in the Kevitsa Ni-Cu-PGE deposit, northern Finland. *Geophysics* **77**, WC149–WC162.

Konstantaki L., Draganov D., Ghose R. and Heimovaara T. 2015b. Seismic interferometry as a tool for improved imaging of the heterogeneities in the body of a landfill. *Journal of Applied Geophysics* **122**, 28–39.

Konstantaki L., Ghose R., Draganov D., Diaferia G. and Heimovaara T. 2015a. Characterization of a heterogeneous landfill using seismic and electrical resistivity data. *Geophysics* **80**, EN13–EN25.

Liu J., Draganov D. and Ghose R. 2018. Seismic interferometry facilitating the imaging of shallow shear-wave reflections hidden beneath surface waves. *Near Surface Geophysics* **16**, 372–382.

Löer K., Meles G., Curtis A. and Vasconcelos I. 2013. Diffracted and pseudo-physical waves from spatially-limited arrays using source-receiver interferometry (SRI). *Geophysical Journal International* **196**, 1043–1059.

Magnusson N.H. 1970. The origin of the iron ores in central Sweden and the history of their alterations. P. 1, Sveriges geologiska undersökning. Serie C, Avhandlingar och uppsatser. Stockholm.

Malehmir A., Durrheim R., Bellefleur G., Urosevic M., Juhlin C., White D.J., et al. 2012. Seismic methods in mineral exploration and mine planning: a general overview of past and present case histories and a look into the future. *Geophysics* **77**, WC173–WC190.

Malehmir A., Holmes P., Gisselø P., Socco L.V., Carvalho J., Marsden P., et al. 2019. Smart Exploration: Innovative ways of exploring for critical raw materials of the EU. 81st EAGE Conference and Exhibition 2019, London, UK, Expanded Abstracts.

Malehmir A., Maries G., Bäckström E., Schön M. and Marsden P. 2017. Developing cost-effective seismic mineral exploration methods using a landstreamer and a drophammer. *Scientific Reports* **7**, 10325.

Malinowski M., Schetselaar E. and White D. 2012. 3D seismic imaging in the Flin Flon VMS mining camp. Part II: forward modeling. *Geophysics* **77**, WC81–WC93.

Manzi M.S.D., Gibson M.A.S., Hein K.A.A., King N. and Durrheim R.J. 2012. Application of 3D seismic techniques to evaluate ore resources in the West Wits Line goldfield and portions of the West Rand goldfield, South Africa. *Geophysics* **77**, WC163–WC171.

Maries G., Malehmir A., Bäckström E., Schön M. and Marsden P. 2017a. Downhole physical property logging for iron-oxide exploration, rock quality, and mining: an example from central Sweden. *Ore Geology Reviews* **90**, 1–13.

Maries G., Malehmir A., Bäckström E., Schön M. and Marsden P. 2017b. Reflection seismic imaging of iron-oxide deposits—An example from Bergslagen mining district of Sweden. 23rd European Meeting of Environmental and Engineering Geophysics, Malmö, Sweden, Expanded Abstracts.

Markovic M., Maries G., Malehmir A., von Ketelholdt J., Bäckström E., Schön M., et al. 2019. Deep reflection seismic imaging of iron-oxide deposits in the Ludvika mining area of central Sweden. *Geophysical Prospecting*.

Mikesell D., van Wijk K., Calvert A. and Haney M. 2009. Virtual refraction: useful spurious energy in seismic interferometry. *Geophysics* **74**, A13–A17.

Place J. and Malehmir A. 2016. Using supervirtual first arrivals in controlled-source hardrock seismic imaging—well worth the effort. *Geophysical Journal International* **206**, 716–730.

Place J., Malehmir A., Högdahl K., Juhlin C. and Nilsson K.P. 2015. Seismic characterization of the Grängesberg iron deposit and its mining-induced structures, central Sweden. *Interpretation* **3**, SY41–SY56.

Roots E., Calvert A. and Craven J. 2017. Interferometric seismic imaging around the active Lalor mine in the Flin Flon greenstone belt, Canada. *Tectonophysics* **718**, 92–104.

Shearer P. 2009. *Introduction to Seismology*. Cambridge University Press.

Snieder R. 2004. Extracting the Green's function from the correlation of coda waves: a derivation based on stationary phase. *Physical Review E* **69**, 46610.

Stephens M. 2009. Synthesis of the bedrock geology in the Bergslagen region, Fennoscandian Shield, south-central Sweden. Sveriges geologiska undersökning (SGU).

Stephens M., Ahl M., Bergman T., Lundström I., Persson L., Ripa M., et al. 2000. Syntes av berggrundsgeologisk och geofysisk information, Bergslagen och omgivande områden, Regional berggrundsgeologisk undersökning. Sammanfattning av pågående undersökningar 1999. ed. Sveriges geologiska undersökning Rapporter och medde – landen 102.

van Dalen K.N., Mikesell T.D., Ruigrok E.N. and Wapenaar K. 2015. Retrieving surface waves from ambient seismic noise using seismic interferometry by multidimensional deconvolution. *Journal of Geophysical Research: Solid Earth* **120**, 944–961.

van Dalen K.N., Wapenaar K. and Halliday D.F. 2014. Surface wave retrieval in layered media using seismic interferometry by multidimensional deconvolution. *Geophysical Journal International* **196**, 230–242.

Verschuur D.J., Berkhout A.J. and Wapenaar C.P.A. 1992. Adaptive surface-related multiple elimination. *Geophysics* **57**, 1166–1177.

Wapenaar K. and Fokkema J. 2006. Green's function representations for seismic interferometry. *Geophysics* **71**, SI33–SI46.

Wapenaar K., Draganov D. and Robertsson J. O. A. Eds. 2008. *Seismic Interferometry: History and Present Status*. SEG Geophysics Reprint Series, Volume 26. SEG, Tulsa, OK.

Xue Y., Aoki N. and Schuster G. 2009. Interferometric prediction and subtraction of surface waves with a nonlinear local filter. *Geophysics* **74**, SI1–SI8.

Yehuwalashet E. and Malehmir A. 2018. Gravity and magnetic survey, modeling and interpretation in the Blötberget iron-oxide mining area of central Sweden. SEG Technical Program Expanded Abstracts 2018: Society of Exploration Geophysicists, 1479–1483.

Yilmaz Ö. 2001. *Seismic Data Analysis: Processing, Inversion and Interpretation of Seismic Data*. SEG, Tulsa, OK.